

# THREE-DIMENSIONAL INDICIAL RESPONSE OF FINITE ASPECT RATIO YAWED WINGS

Carlos E. Manglano-Villamarin and Scott T. Shaw  
School of Engineering, Cranfield University  
Cranfield, United Kingdom

## Abstract

A study of the indicial response of finite aspect ratio yawed wings has been conducted. The indicial response was obtained directly from solutions of the unsteady Euler equations for two- and three-dimensional wings subjected to a step change in incidence.

The computed data reveal several important characteristics in the behaviour of the unsteady response of three-dimensional wings. The initial response is shown to be independent of both aspect ratio and yaw confirming the results of linearized theory. During the subsequent development of the unsteady response significant differences are observed between the two- and three-dimensional behaviours as a consequence of changes to both wing aspect ratio and yaw angle. These differences cannot be explained entirely through simple sweep theory or shaping of the local lift curve slope distribution. The formation and spanwise propagation of acoustic waves is shown to have a significant influence on the development of the unsteady forces and moments, while for yawed wings it is shown that changes in the way that the windward and leeward tip vortices form are also important.

It is concluded that current industrial approaches based upon the use of two-dimensional indicial response functions may be unreliable.

## Nomenclature

b	Semi-span
$C_N$	lift coefficient
$C_m$	pitching moment coefficient
$C_p$	pressure coefficient
E	energy
F	numerical flux
i	cell index
L	characteristic length scale
M	Mach number
n	surface unit normal
P	pressure
q	pitch rate
Q	conserved variables
R	residual
t	time
s	non-dimensional time
S	surface area
u, v, w	Cartesian components of local velocity
V	freestream velocity
x, y, z	Cartesian co-ordinate system
$\Omega$	Volume

$\alpha$	incidence angle (degrees)
$\gamma$	ratio of specific heats (1.4 for air)
$\kappa$	coefficient in MUSCL scheme
$\lambda$	sweep angle (degrees)
$\rho$	fluid density
$\tau$	pseudo-time

## Introduction

Accurate modelling of the unsteady aerodynamic loads generated by the helicopter main rotor during forward flight is important in understanding vehicle aerodynamic performance, vibration and aero-acoustics. Although it is possible to simulate unsteady flows around aerodynamic bodies directly through solutions of the Navier-Stokes equations the difficulty of the task faced, particularly when the problem involves a strong non-linear coupling between the unsteady motion and the fluid dynamics, is such that some compromise must be made between overall accuracy and the cost of obtaining solutions.

The cost of generating numerical solutions of the partial differential equations that govern fluid flow and recognition that much of the resulting information, such as field data, may not be required in a design context has motivated the study of high-fidelity reduced order modelling techniques that accurately capture the behaviour of the unsteady forces and moments at significantly reduced expense.

Reduced order modelling approaches based on inexpensive quasi-steady representations of the aerodynamics have proven inadequate for predicting loads and moments on manoeuvring bodies. This is because they fail to account for the influence of important physical phenomena such as interactions with the shed vortical wake and the propagation of acoustic pressure disturbances generated at the body surface. Classical indicial theory provides an inexpensive but rigorous mathematical approach to the modelling of these unsteady phenomena.

The indicial function is a mathematical concept that relates the unsteady response of a system to excitation in a particular degree of freedom. They are obtained by considering the response of a system to a step excitation applied instantaneously and then held constant. Once the indicial functions of the system are known the response to arbitrary excitations can be obtained in a cost effective manner using linear superposition and convolution.

The classical indicial theory is based on the assumption that the aerodynamic response is independent of the prior motion history and is determined completely by the current forcing. Thus the indicial response of pitching moment to a step variation in pitch rate can be defined fully as,

$$C_{m_q}(t, \tau) = \lim_{\Delta\left(\frac{qL}{V}\right) \rightarrow 0} \frac{\Delta C_m(t, \tau)}{\Delta\left(\frac{qL}{V}\right)} \quad (1)$$

This linearization has proven to be robust provided that the topology of the flow is unchanged by the forcing. The theory has subsequently been extended to include the influence of compressibility and unsteady separation through the use of physics based inference models and empirical data, see for example Beddoes [Ref 1,2].

Unfortunately closed form analytical expressions for the indicial functions of interest in external aerodynamics can only be determined for inviscid, incompressible, irrotational flows. A range of empirical techniques have been developed that provide a means of extracting indicial response functions from physical and computational experiments. Leishman [Ref 3] has presented techniques for identifying indicial functions from oscillatory experiments, while Sitaraman and Baeder [Ref 4] proposed using computational fluid dynamics to extract indicial models directly from impulse responses. Shaw and Qin [Ref 5,6] independently proposed the use of step inputs to obtain indicial functions for both pitch and in-plane responses and have shown that the resulting models are almost identical with those obtained from oscillatory data. They also proposed models that included a weak dependence on the time history of the motion through the use of motion dependent model coefficients.

Alternative approaches to the reduced order modelling of unsteady aerodynamics include the contributions of Gaitonde and Jones [Ref 7] who have developed model identification techniques, intended for use in state-space modelling that are based upon numerical solutions of the linearized Euler equations. These models can easily be recast in a form suitable for use in indicial modelling. Beedy et al [Ref 8] have shown how CFD can be used to populate the ONERA dynamic stall model which requires the solution of a simple ordinary differential equation.

Even in the absence of three-dimensional planform variation the flow experienced by rotor blades in forward flight is highly three-dimensional. This is illustrated in Fig. 1 which shows local sweep contours for a rectangular blade at a modest forward flight speed. Beddoes has developed a sophisticated

physics based approach for three-dimensional rotor simulations incorporating two-dimensional indicial response functions, a free wake model [Ref 9] and elements of classical wing theory for the effects of sweep and aspect ratio [Ref 10,11]. This method has been exercised for a range of problems and appears to provide credible results that could be used within a rotor design [Ref 10, 11,12].

Singh and Baeder [Ref 13] computed the indicial response of unswept finite aspect ratio wings and concluded that there was a simple relationship between the 3D response and the response functions of the wing section. More recently Sitaraman and Baeder [Ref 14] extended these ideas by combining computed 2D response functions with a simplified aerodynamic representation of fixed and rotating wings to compute blade vortex interactions on three-dimensional lifting surfaces.

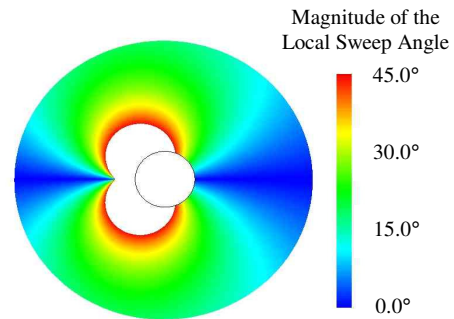


**Fig 1. Local Sweep in Forward Flight**

Despite the progress that has been made in applying indicial theory to increasingly complex motions, geometry and physics the nature of the response functions in three-dimensional flows remains poorly understood. Although Singh and Baeder [Ref 13] had suggested that it should be possible to model three-dimensional flows using two-dimensional response functions and the local lift curve slope this was not demonstrated. Indeed, examination of their computed data suggests that not only is the amplitude modified by three-dimensional effects, but also the basic form of the response. Accepting this observation then the use of two-dimensional response as the underpinning conceptual model in three-dimensional methods remains a significant weakness.

The objective of this paper is to explore in detail the indicial response of finite aspect ratio yawed wings. Particular attention is paid to the form of the computed response and how this is modified by three-dimensional effects. This is achieved through the numerical solution of the unsteady three-dimensional Euler equations for aerofoils and wings subjected to a step change in incidence. Results are

presented that assess both the effects of aspect ratio and the effects of sweep on the unsteady response.

### Numerical Model

#### Governing Equations

The equations governing the flow of an unsteady, inviscid, iso-thermal fluid are the three-dimensional Euler equations. This system of equations can be written for a domain  $\Omega$  with boundary  $dS$  using an arbitrary Lagrangian-Eulerian frame of reference (ALE) in the following conservative integral form,

$$\frac{\partial}{\partial t} \iiint_{\Omega} Q d\Omega + \iint_S F \cdot n dS = 0 \quad (2)$$

The vector of conserved variables  $Q$  and the flux vector  $F$  are determined from,

$$Q = \begin{bmatrix} \rho \\ \rho u \\ \rho v \\ \rho w \\ \rho E \end{bmatrix} \quad \text{and} \quad F = \begin{bmatrix} \rho \bar{U} \\ \rho \bar{U} u + P \cdot n_x \\ \rho \bar{U} v + P \cdot n_y \\ \rho \bar{U} w + P \cdot n_z \\ \rho \bar{U} E + \tilde{U} P \end{bmatrix} \quad (3)$$

In these equations  $n_i$  are the Cartesian components of the outward pointing unit vector normal to the surface.  $\tilde{U}$  is the velocity normal to the element surface and  $\bar{U}$  is the contra-variant velocity given by,

$$\bar{U}_i = u_i - \frac{dx_i}{dt} \quad (4)$$

where  $u_i$  are the components of the absolute velocity and  $\frac{dx_i}{dt}$  are the components of the grid velocity. In order to close this system of equations the fluid is considered to be an ideal gas and the density, pressure and energy per unit mass are related to one another through the equation of state,

$$\frac{P}{\rho} = (\gamma - 1) \left[ E - \frac{1}{2} u^2 \right] \quad (5)$$

the working fluid is assumed to be a di-atomic gas with a ratio of specific heats  $\gamma = 1.4$ .

#### Boundary Conditions

At the surface of the body subsonic outflow is assumed. A no penetration condition is imposed on the velocity vector at the solid surface and the remaining variables are extrapolated from values within the computational domain. At the far-field

boundary characteristic based non-reflecting boundary conditions determined from an approximate solution of the Riemann boundary value problem [Ref 15] are employed.

### Numerical Method

#### Spatial Discretization

The governing equations are solved using an unstructured cell-centred finite volume scheme. The discrete equations for cell  $i$  are of the form,

$$\sum_{m=1}^M \tilde{f}_m(Q)(n \cdot S)_{i,m} = Q_i \Omega_i \quad (6)$$

here  $\tilde{f}_m(Q)$  is the inter-cell flux through face  $m$  and  $M$  is the number of faces defining cell  $i$ . The numerical flux is evaluated using the approximate Riemann solver described by Osher and Solomon [Ref 16] with modifications that account for the changed eigenvalues of the governing equations in the moving frame of reference, see Shaw [Ref 17].

To enhance the spatial resolution of the method the left and right states are evaluated using a nominally third-order accurate upwind biased interpolation scheme based upon the work of van Leer [Ref 18]. For the interface between cells  $i$  and  $j$  the left and right hand states are calculated from,

$$Q_L = Q_i + \frac{1}{4} \left[ (1 - \kappa) \tilde{\Delta}_i^- + (1 + \kappa) \tilde{\Delta}_i^+ \right] \quad (7)$$

$$Q_R = Q_j + \frac{1}{4} \left[ (1 - \kappa) \tilde{\Delta}_j^+ + (1 + \kappa) \tilde{\Delta}_j^- \right]$$

in which  $\tilde{\Delta}_i^+$  and  $\tilde{\Delta}_i^-$  are estimates of the solution gradient in cell  $i$  based upon forwards and backwards difference operators. A value for  $\kappa$  of 1/3 results in a third-order interpolation scheme. To avoid spurious oscillations in the vicinity of discontinuities slope limiters are employed that reduce the spatial accuracy of the scheme to first-order.

#### Temporal Discretization

Following spatial discretization a system of ordinary differential equations of the form,

$$\frac{dQ_i \Omega_i}{dt} = -R_i(Q) \quad (8)$$

is obtained. This system of equations is marched in time using a second-order implicit scheme,

$$\frac{3Q_i^{n+1} - 4Q_i^n + Q_i^{n-1}}{2} = \frac{\Delta t}{\Omega_i} R_i(Q^{n+1}) \quad (9)$$

A fictitious time derivative is introduced in Equation (9) and the resulting system is marched to a converged solution in pseudo-time using a first-order explicit scheme at each global time step. Local pseudo-time stepping is employed to accelerate convergence to the solution of the implicit system.

The resulting numerical scheme is third-order in space and second-order in time in smooth regions of the flow and first-order in space and second-order in time in the proximity of large flow gradients, such as shock waves.

### Parallel Implementation

The numerical method described in the previous sections has been parallelized by partitioning the domain into several smaller sub-domains. The domain decomposition is performed on the graph of the unstructured grid using the MeTiS software [Ref 19] Communication between the domains, which are assigned to individual processors within the parallel computing environment, is achieved using the MPI message passing library.

### Verification

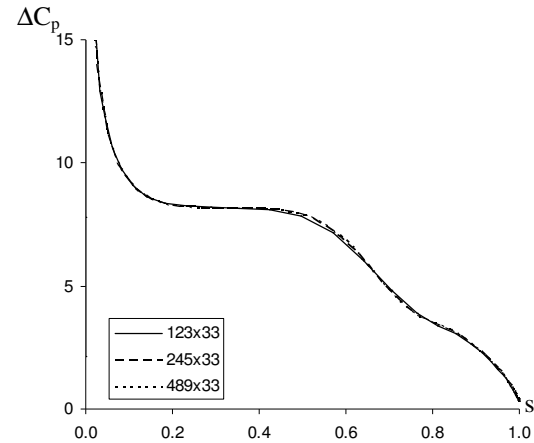
In an effort to demonstrate the suitability of the model for its intended application, computations of the two-dimensional indicial response of NACA 0006 and NACA 0012 airfoils to step changes in heave were performed. Initially steady results were obtained at an incidence of  $0^\circ$  and  $5^\circ$  for Mach numbers in the range  $0.2 \leq M \leq 0.7$ . Unsteady computations were then performed at heave velocities corresponding to a step change of  $1^\circ$  and  $2^\circ$  of incidence using the steady data as initial conditions.

### Convergence Studies

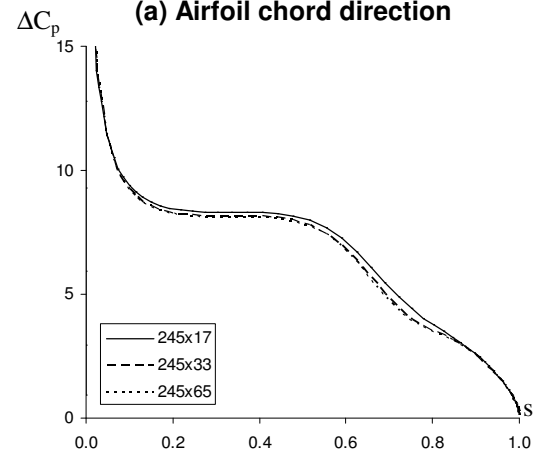
A grid convergence study was performed for both the steady and unsteady solutions following the method proposed by Roache [Ref 20]. The effect of grid refinement in the chord-wise and airfoil normal directions was investigated independently. In the chord-wise direction grids having 489, 245 and 123 nodes were studied with 33 points in the normal direction, while in the normal direction grids of 65, 33 and 17 nodes were investigated with 245 points around the airfoil. Grid points were distributed to capture the expected gradients at the stagnation point, trailing edge and close to the airfoil surface. In all cases the grid extended at least 15 chord lengths from the aerofoil surface in all directions.

Analysis of the steady data and initial impulse response show that the solutions lie within the asymptotic range with an observed order of accuracy slightly greater than the nominal order of accuracy of the numerical method. Computed pressure loadings shortly after the application of the step response ( $s = 0.391$ ) are shown in Fig. 2. Large variations in the

computed solution between grids with 17 and 33 points in the normal direction are observed, while the computed solution is largely insensitive to the number of points around the airfoil. The data suggest that a grid having 245 points around the airfoil and 33 points in the airfoil normal direction is sufficient for the current class of problems. All subsequent computations were performed on grids having these dimensions.



(a) Airfoil chord direction



(b) Airfoil normal direction

**Fig 2. Influence of grid resolution on computed pressure loading  $s = 0.391$ , NACA 0006 aerofoil,  $M = 0.3 \alpha = 0^\circ + 1^\circ$**

The sensitivity of the computed data to time step was also investigated. Five different time steps using a refinement ratio of 2 were employed. Care was taken to ensure that iterative convergence was achieved during the pseudo-time iterations. Following the analysis of Roache [Ref 20] the error due to the temporal truncation error was estimated to be approximately 1% for the coarsest time step. This level of error was deemed to be acceptable and all subsequent computations were performed with a time step that was half of the coarsest time step considered.

### Initial Response

The initial aerodynamic response of an aerofoil of zero thickness to a step change in incidence can be determined exactly using piston theory,

$$\frac{C_N(0^+)}{\Delta\alpha} = \frac{4}{M} \quad (10)$$

see for example Beddoes [Ref 1]. As the numerical method requires a finite time-step it is not possible to compute the solution at  $s = 0^+$  directly, instead results from the initial two steps were extrapolated to time  $s = 0^+$ . The exact solution is compared with the computations for the NACA 0006 aerofoil in Fig. 3. Good overall agreement is observed between the computed and theoretical values, the small over-prediction in the CFD solutions at low Mach numbers is attributed to the finite thickness of the aerofoil used in the numerical computations. At the higher Mach numbers the linearized theoretical analysis is no longer applicable and consequently the presence of shock waves in the numerical simulations leads to an increasingly large discrepancy.

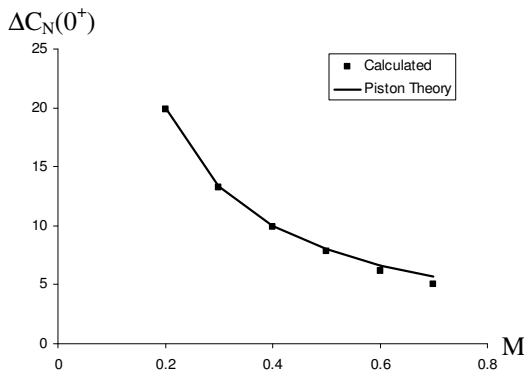


**Fig 3 Comparison of analytical and computed initial response to a step change of incidence, NACA 0006 aerofoil,  $M = 0.3 \alpha = 5^\circ + 2^\circ$**

Lomax [Ref 21] used the linearized Euler equations to derive exact closed-form expressions of the compressible indicial response of a flat plate aerofoil to a step change in incidence. Lomax presented results for both the change in lift,

$$\frac{\Delta C_N(s)}{\Delta\alpha} = \frac{4}{M} \left( 1 - \frac{1-M}{2M} s \right) \quad (11)$$

and the change in pressure distribution,

$$\frac{\Delta C_p(x, \hat{t})}{\Delta\alpha} = \Re \left[ \begin{array}{l} \frac{8}{\pi(1+M)} \sqrt{\frac{\hat{t}-x'}{M\hat{t}+x'}} + \\ \frac{4\pi}{M} \cos^{-1} \left( \frac{\hat{t}(1+M) - 2(c-x')}{\hat{t}(1-M)} \right) - \\ \frac{4\pi}{M} \cos^{-1} \left( \frac{2x' - \hat{t}(1-M)}{\hat{t}(1+M)} \right) \end{array} \right] \quad (12)$$

with  $x' = x - M\hat{t}$  and  $\hat{t} = \frac{s}{2M}$  for the period of time  $0 < s \leq \frac{2M}{1+M}$ .

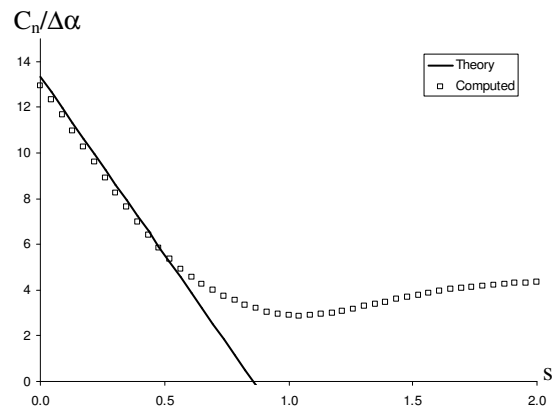


**Fig 4 Comparison of analytical and computed lift response to a step change of incidence, NACA 0006 aerofoil,  $M = 0.3 \alpha = 0^\circ + 1^\circ$**

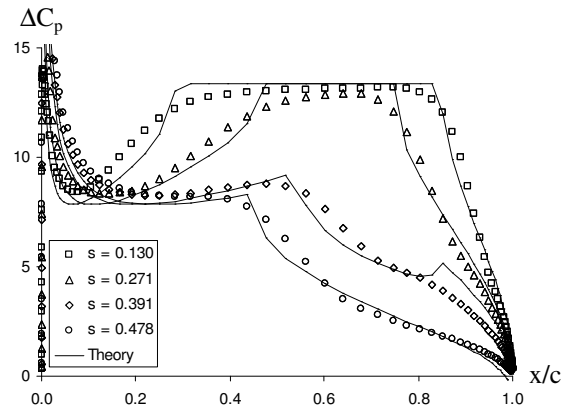


**Fig 5 Comparison of analytical and computed pressure response to a step change of incidence, NACA 0006 aerofoil,  $M = 0.3 \alpha = 0^\circ + 1^\circ$**

Computed lift data are compared with the exact result for the NACA 0006 aerofoil in Fig. 4 at a Mach number  $M = 0.3$ . Although the peak response is not captured exactly by the computed data for the reasons discussed earlier, the subsequent decay rate closely approximates the theoretical result. This

comparison indicates that the initial lift decay is well represented by the computed solution.

Computed surface pressure distributions at several instants in time following the forcing are compared with the analytical solution in Fig. 5. Agreement with the linearized theory is considered to be fair. The discrepancies that are observed are related to two-dimensional effects, in particular the finite thickness and surface curvature of the aerofoil used for the computations, that are not represented in the theoretical analysis. The curvature of the aerofoil causes refraction of the acoustic waves, which are considered planar in the theory, leading to a poor prediction of the phase. The present data are comparable with those obtained by other authors for this problem; see for example Singh and Baeder [13].

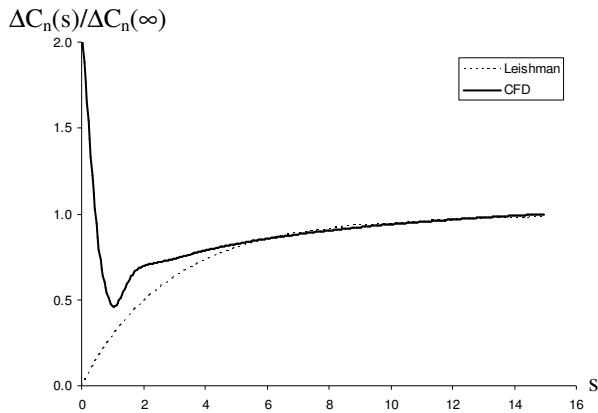


**Fig 6. Comparison of empirical and computed lift response to a step change of incidence, NACA 0012 aerofoil,  $M = 0.3 \alpha = 0^\circ + 1^\circ$**

A short time after the forcing is applied the lift response of the aerofoil is dominated by the transport of vorticity shed into the wake. This so called circulatory response has been determined empirically by Leishman from oscillatory test data, see [Ref 3] for further details. Leishman approximates the response by an exponential series of the form,

$$\frac{\Delta C_n(s)}{C_{n\alpha} \Delta\alpha} = (1.0 - 0.918e^{-0.366s} + 0.082e^{-0.102s}) \quad (13)$$

Fig. 6 presents a comparison of the computed data and Leishman's approximation for a Mach number of 0.2. Clearly the computation is in poor agreement with Leishman's result in the initial phase of the response. But once the influence of the impulsive loading becomes negligible excellent agreement is found between the empirical and numerical models.

## Results

Having established that the MERLIN flow solver was suitable for its intended application it was then used to investigate the unsteady response of finite aspect ratio yawed wings subject to step changes in incidence. During the study 12 rectangular wings of differing aspect ratio and yaw were investigated, details are provided in Table 1, at a range of Mach numbers and incidences. The wings, based on the NACA 0012 aerofoil, were untwisted and had a straight cut at the tip.

Grids were generated based upon the two-dimensional meshes discussed above. An unstructured grid was generated on the wing tip surface and merged with the existing two-dimensional aerofoil grid. The resulting mesh was then extruded in the span-wise direction to obtain a three-dimensional mesh. The grid was clustered towards the wing tips to provide resolution of the expected tip-vortices. The resulting grids have a total of 33, 33 and 65 nodes in the spanwise direction for the aspect ratio 3, 6 and 20 wings respectively. The grids extend 15 chord lengths from the wing tips.

Aspect Ratio	3	6	20
Yaw ( $^\circ$ )			
0	Wing 1	Wing 2	Wing 3
15	Wing 4	Wing 5	Wing 6
30	Wing 7	Wing 8	Wing 9
45	Wing 10	Wing 11	Wing 12

**Table 1. Detail of aspect ratio and yaw angle of the wings considered in the study**

The three-dimensional computations discussed in the present paper were performed at a Mach number of  $M = 0.2$  and initial incidences of  $\alpha_0 = 5^\circ$  and  $\alpha_0 = 7^\circ$ . The pitch forcing was applied by rotating the grid about the quarter chord point. Computed data were obtained for step changes of  $\Delta\alpha = +2^\circ$  and of  $\Delta\alpha = -2^\circ$ . Converged steady solutions were obtained at the initial incidence and the resulting data was then used to compute the unsteady flow around the wing at an incidence of  $\alpha = \alpha_0 + \Delta\alpha$ .

### Total Lift Response

The computed total lift response to a step change in incidence is presented in Fig. 7 for the aspect ratio 6 wings considered in the present study. The calculated data were obtained for a Mach number of  $M = 0.2$  and an incidence of  $\alpha = 5^\circ + 2^\circ$ .

The unsteady development of the lift mirrors that observed for the two-dimensional wing. Initially,  $0 < s < 0.25$ , there is an impulsive disturbance related to the generation of the starting acoustic waves and their associated reflections from the leading and trailing edges and wing tips. The initial decay of the

impulsive loading is linear as predicted by theory for infinite chord finite span wings, see the discussion of Tobak [Ref 22]. At later times,  $s > 1.0$ , the lift history is dominated by the influence of the shed vorticity. The shed vorticity reduces the effective incidence experienced by individual wing sections, but as the vorticity is transported downstream its influence diminishes allowing the lift to asymptote towards the new steady value.

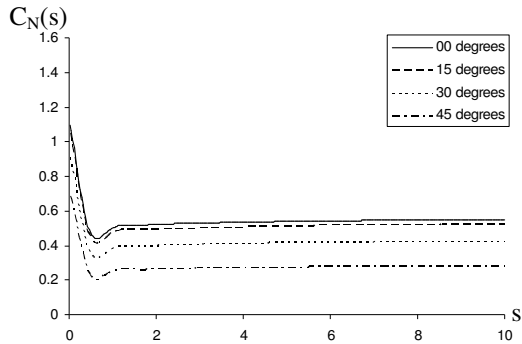


Fig 7. Total lift response (aspect ratio 6)

The initial response,  $s = 0^+$  is presented in Fig. 8. This value was obtained using linear extrapolation between the computed values at the first two time-steps. At constant yaw angle the computed data are independent of aspect ratio, while at constant aspect ratio the initial response is seen to depend upon the yaw angle, diminishing as yaw is increased. If the computed values are adjusted in line with simple sweep considerations the data are observed to collapse to a single value (the difference between the largest and smallest values is approximately 0.3%). This behaviour is expected from simple acoustic considerations and the computed values are in favourable agreement with the result predicted using piston theory. As for the two-dimensional case the discrepancies observed between the computed and theoretical results are attributed to two- and three-dimensional flow, in particular the effects of finite thickness and the tip vortices.

The circulatory response of the wings can be explored in further detail by examining the ratio of the unsteady change in lift to the difference between the initial and final steady state values. This ratio, which at later times is equivalent to the circulatory response function, is presented in Fig. 9 for unswept wings of aspect ratio 3, 6 and 20.

The effect of aspect ratio on the total computed response is substantial. As might be expected from simple physical considerations the computed data tend towards the two-dimensional result as aspect ratio is increased, but only in the latter stages of the response. At earlier times there are clear differences in behaviour even for the relatively high-aspect ratio wing. These differences can be partially explained in terms of the phenomena already observed in the two

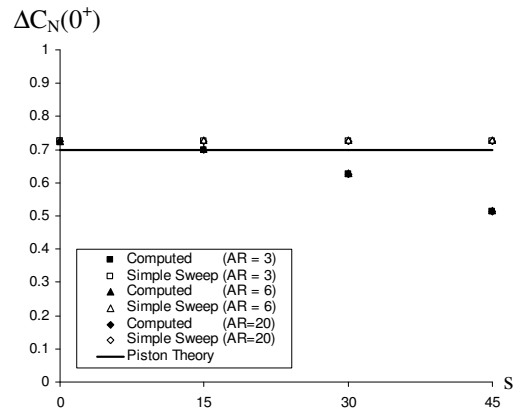


Fig 8. Total computed initial lift response,

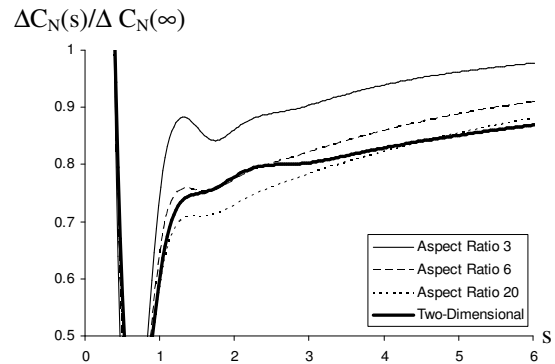


Fig 9. Variation of computed circulatory response with aspect ratio ( $\lambda = 0^\circ$ )

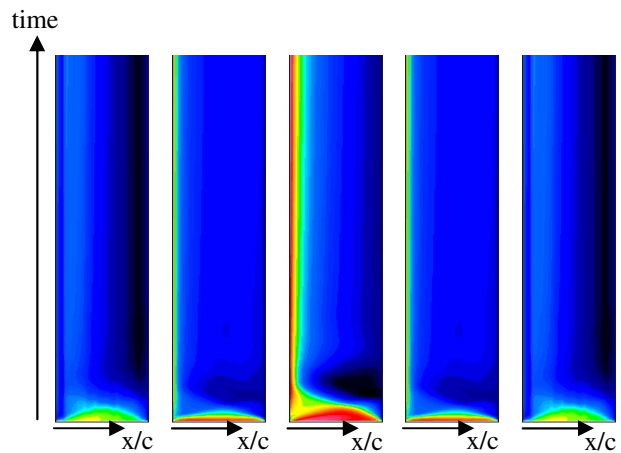
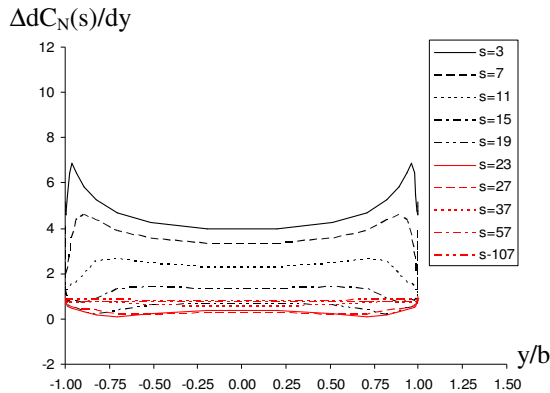


Fig 10. Variation of chordwise loading with time (aspect ratio 6,  $\lambda = 0^\circ$ )

dimensional case. The chordwise propagation of pressure waves can be clearly seen in the contours of unsteady pressure loading  $\Delta(C_{P_{\text{upper}}} - C_{P_{\text{lower}}})$  presented in Fig. 10. Of note is the more rapid response in the vicinity of the tips compared to that observed at the centre section. This is attributed to the development of additional acoustic disturbances along the wing tip that propagate inboard and is

illustrated more clearly in Fig.11 which shows the spanwise variation of loading at the centre chord for several instants in time.



**Fig 11. Development of spanwise lift distribution for the unswept aspect ratio 6 wing**

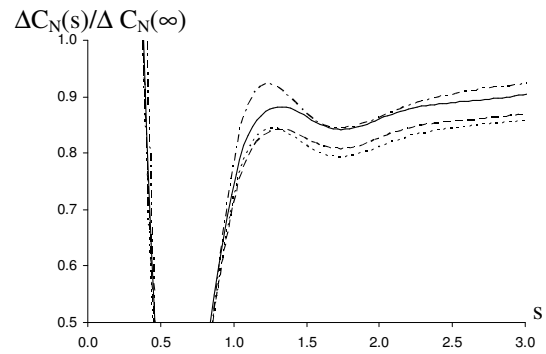
The effect of yaw angle on the computed circulatory response is presented in Fig. 12 for the wings of aspect ratio 3, 6 and 20. The behaviour is complex and strong coupling between aspect ratio and yaw angle is evident.

#### Local Lift Response

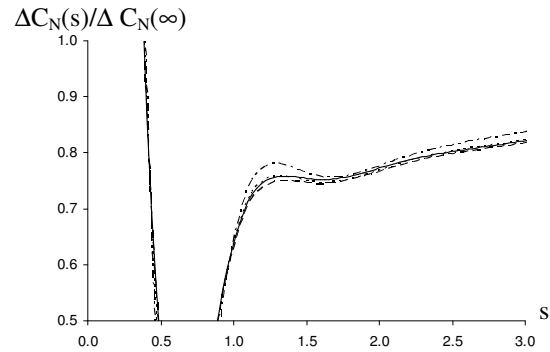
The results presented thus far suggest that while simple theory can be used to describe the variation of local lift curve slope the common assumption that the response function itself is independent of planform geometry is flawed. That this is the case can be demonstrated by studying the response at individual spanwise locations. This is done in Fig. 13 and 14 which provides computed response functions for the aspect ratio 6 wing at various yaw angles.

At 0° yaw the local response over most of the wing exhibits similar behaviour to that of the two-dimensional aerofoil. As yaw angle is increased significant differences develop in the local response at the windward and leeward tips, Fig. 13 and Fig. 14 respectively.

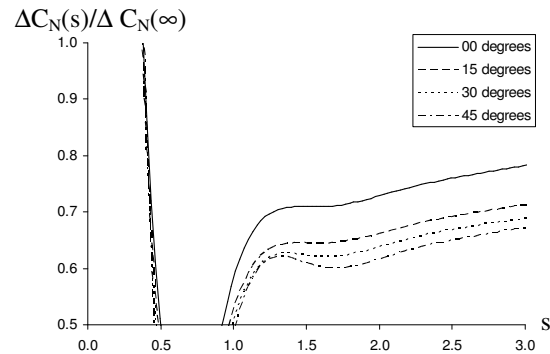
Fig. 15 shows comparisons of local initial response immediately following application of the forcing with the value predicted by piston theory for the aspect ratio 6 wings at several yaw angles. The data over the centre sections require no comment, but closer to the wing tips piston theory is observed to breakdown. This behaviour can be attributed to strong local three-dimensional effects induced by the presence of the wing tip vortices. Yawing the wing leads to asymmetric behaviour at the windward and leeward tips; At the windward tip there is a significant growth in the region influenced by the tip as yaw angle is increased, while at the leeward tip the initial response is largely insensitive to changes in yaw angle.



**(a) Aspect ratio 3**



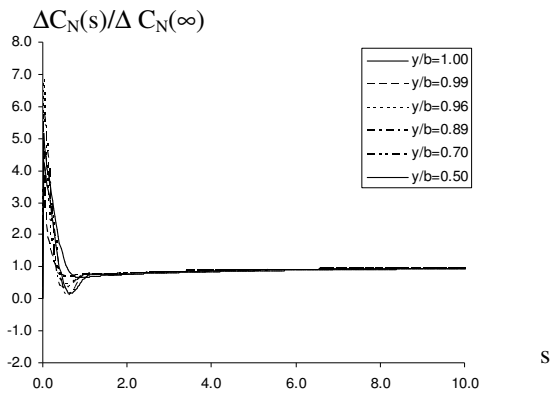
**(b) Aspect ratio 6**



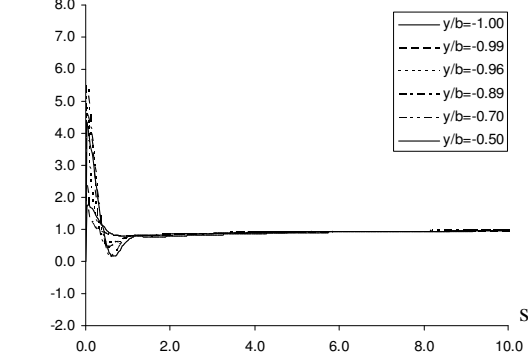
**(c) Aspect ratio 20**

**Fig 12. Variation of computed circulatory response with yaw angle**

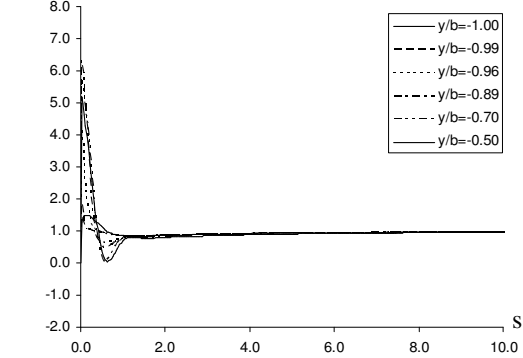
The initial rate of decay is found to be independent of both wing aspect ratio and yaw angle. This is illustrated in Fig. 16 for the aspect ratio 6 wing at a yaw angle of 0° and in Fig. 17 for a yaw angle of 30°. Although the initial decay of the impulse response is seen to be independent of planform geometry at later times the impulse responses diverge, this is most evident in the response presented at  $y/b = 0.70$  and  $y/b = 0.50$  for the straight wing. The length of time between the forcing and the time at which the decay rates diverge can be correlated with distance from the wing tip implicating spanwise propagation of acoustic waves as the most likely physical explanation for the observed behaviour. This



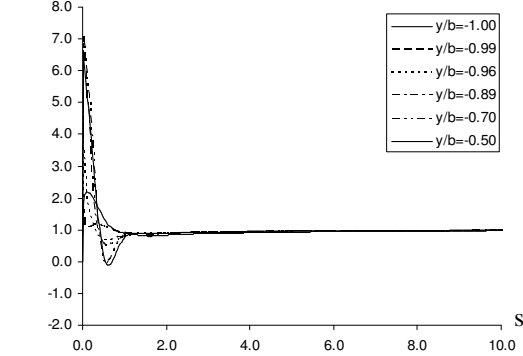
(a)  $\lambda = 0^\circ$



(b)  $\lambda = 15^\circ$

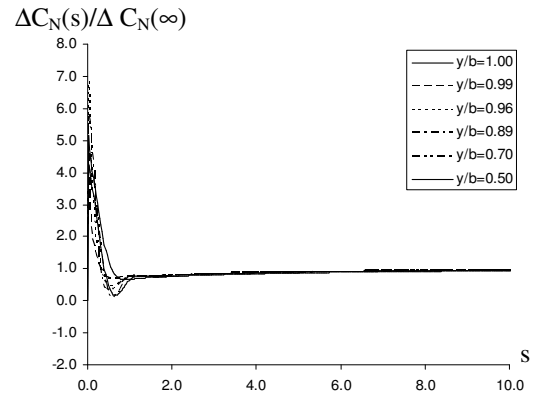


(c)  $\lambda = 30^\circ$

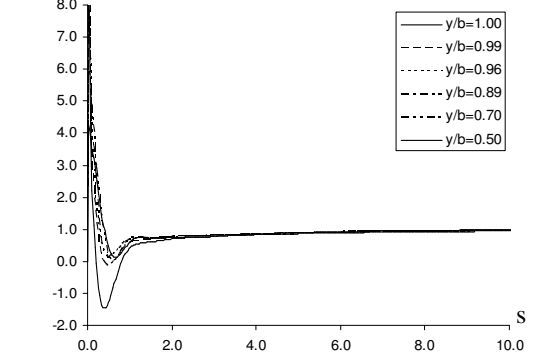


(d)  $\lambda = 45^\circ$

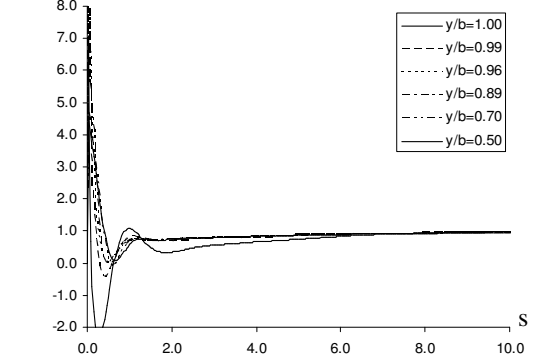
**Fig. 13** Spanwise variation of the computed lift response,  $M = 0.3$  and  $\alpha = 5^\circ + 2^\circ$  (windward tip)



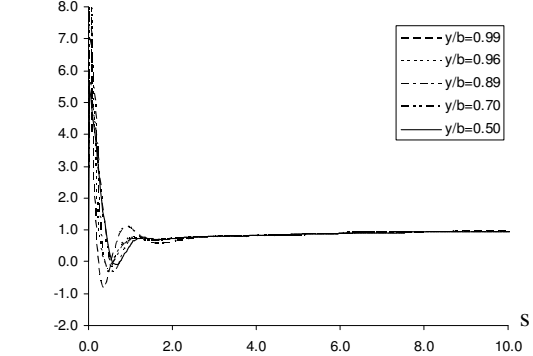
(a)  $\lambda = 0^\circ$



(b)  $\lambda = 15^\circ$



(c)  $\lambda = 30^\circ$



(d)  $\lambda = 45^\circ$

**Fig. 14** Spanwise variation of the computed lift response,  $M = 0.3$  and  $\alpha = 5^\circ + 2^\circ$  (leeward tip)

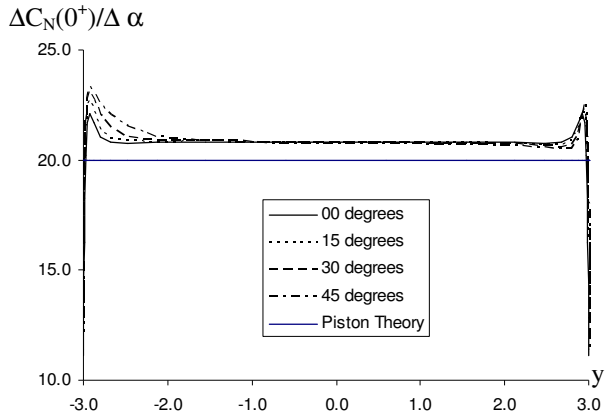


**Fig 15. Variation of local initial response with yaw angle (aspect ratio 6 wing)**

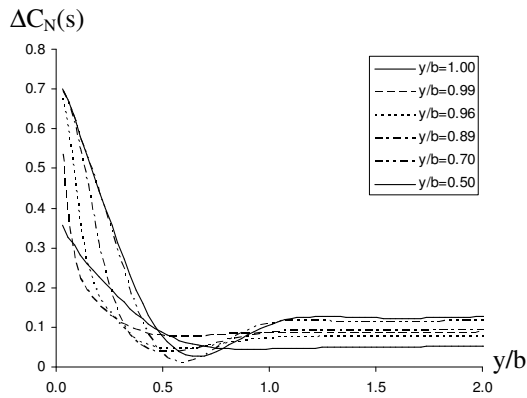


**Fig 16. Comparison of local initial response at the wing tips (aspect ratio 6 wing, λ = 0°)**

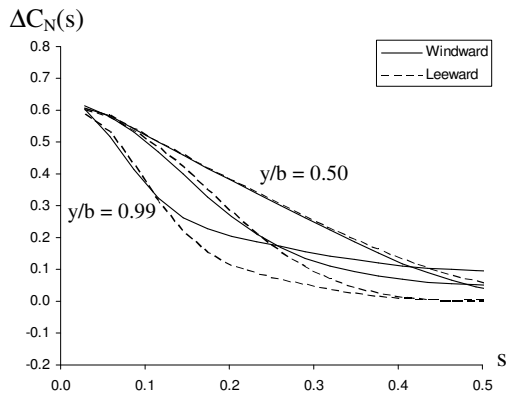


**Fig 17. Comparison of local initial response at the wing tips (aspect ratio 6 wing, λ = 30°)**

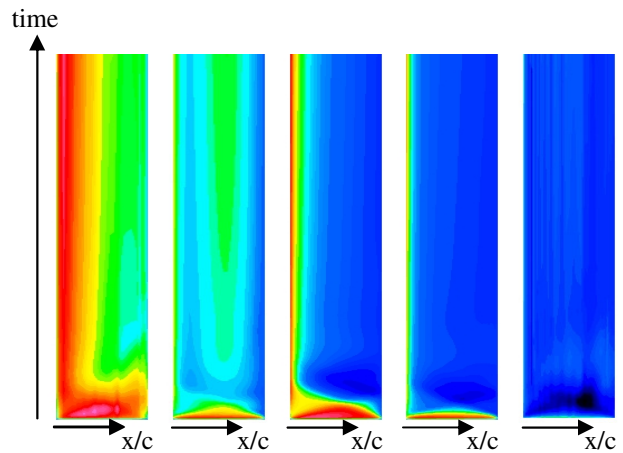
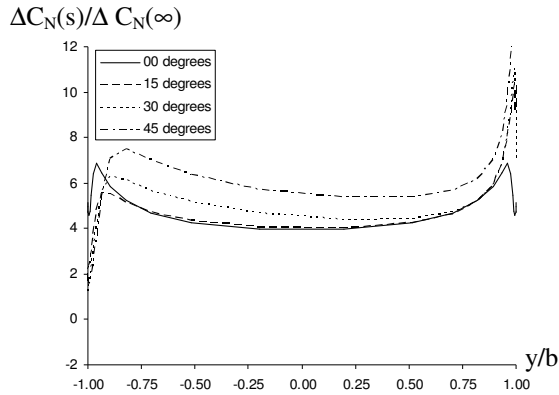


**Fig 17. Variation of chordwise loading with time (aspect ratio 6, λ = 30°)**

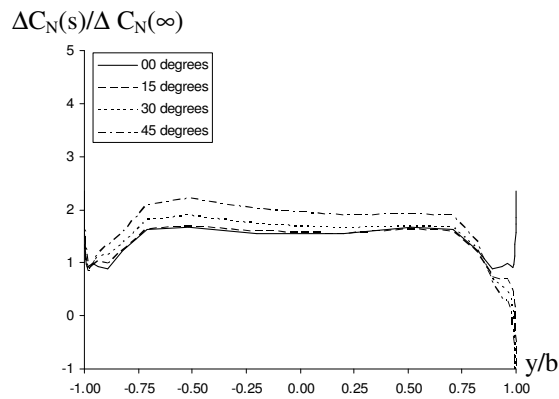
hypothesis is supported by visualizations of the computed loading distribution, Fig. 18.

The results presented at  $y/b = 0.99$ ,  $y/b = 0.89$  and  $y/b = 0.50$  for the yawed wing, Fig. 17, suggest that there is some influence of yaw angle on the generation and propagation of the spanwise acoustic disturbances. In an effort to understand this behaviour further the spanwise loading variation was studied. Fig. 18 presents spanwise distributions of lift at three instants in time. The selected data correspond to instances of initial, transitional and circulatory behaviour. The presented data confirm the presence of strong three-dimensional effects at the tips. At zero yaw angle the development of the tip vortices provides a local increase in effective incidence with an associated local variation of lift. An increasingly asymmetric lift distribution is produced as yaw angle is increased. This variation is related to changes in the way the tip vortex is formed. At the windward tip, which projects into the oncoming freestream, the formation of the tip vortex is disrupted by the presence of stagnating flow on the wing tip. Two distinct vortical structures develop on the upper and lower surfaces at the wing tip. These structures pass across the planform into the wake where they roll up into a single vortex. At the leeward tip, which projects out of the flow, a single vortex is formed that separates from the geometry close to the point of maximum thickness. The development of the windward and leeward tip vortices is visualized at the initial steady flow conditions in Fig. 19 for the aspect ratio 6 wing at a yaw angle of 30°.

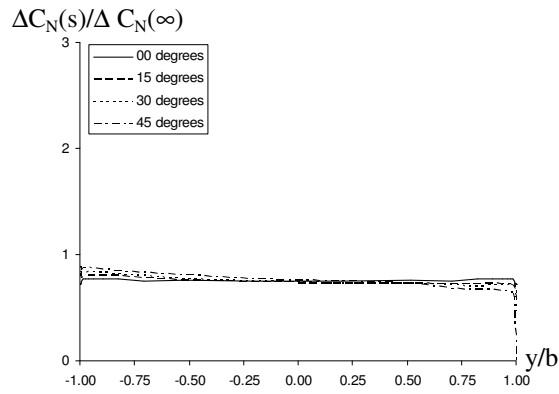
The circulatory response is illustrated for the aspect ratio 6 wing in Fig. 20 and Fig. 21 for yaw angles of 0° and 30° respectively. The data show significant influence of both aspect ratio and yaw. The data can be fitted using an exponential function of the form,



(a)  $s = 0.12$  (initial)

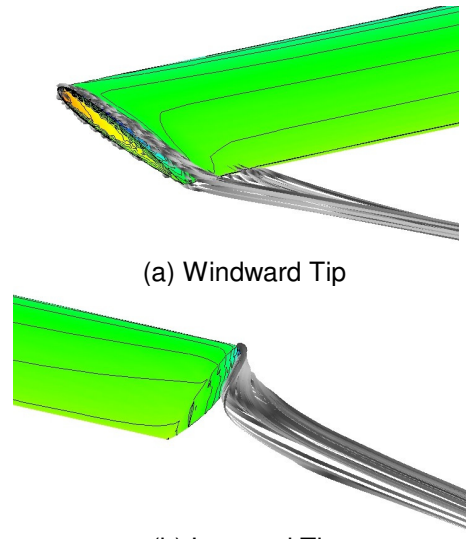


(b)  $s = 0.41$  (transitory)



(c)  $s = 1.57$  (circulatory)

**Fig 18. Spanwise Lift Distribution,  $M = 0.2$  and  $\alpha = 5^\circ + 2^\circ$**



(a) Windward Tip

(b) Leeward Tip

**Fig. 19 Visualization of tip vortex formation on the aspect ratio 6 wing,  $\lambda = 30^\circ$**

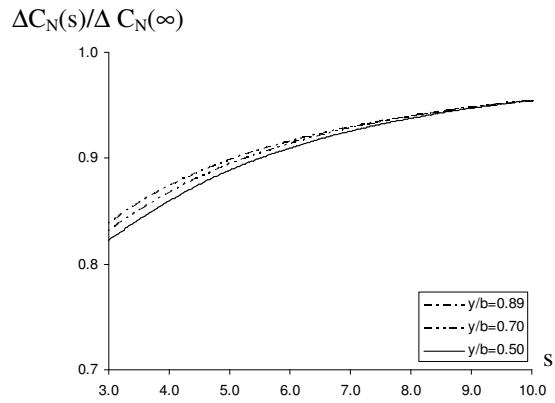


**Fig. 20 Computed circulatory response, aspect ratio 6 wing,  $\lambda = 0^\circ$**

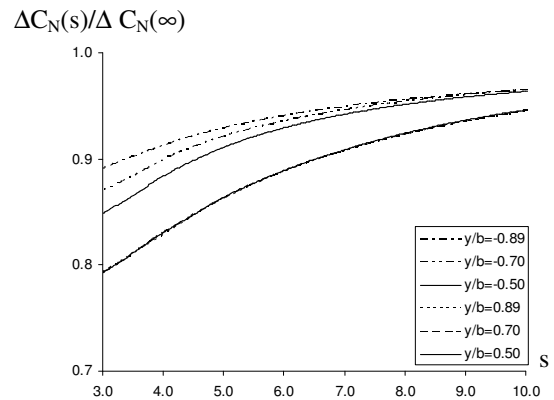


**Fig. 21 Computed circulatory response, aspect ratio 6 wing,  $\lambda = 30^\circ$**

$$\frac{\Delta \frac{d}{dy} C_n(s)}{\Delta \frac{d}{dy} C_n(\infty)} = (1.0 - A_1 e^{-b_1 s} + (0.5 - A_1) e^{-b_2 s}) \quad (14)$$

which is of a similar functional form to the well known Wagner function [Ref 1]. For the straight wing the exponential terms are of constant magnitude,  $A_1 = 0.13$  provides an acceptable fit and there is little variation of the coefficient  $b_1$ , see Table 2. The variation of coefficient  $b_2$  is more pronounced. On the outboard section of the wing the variation is nearly linear and approaches a value of 0.4 at the centre section.

y/b	$b_1$	$b_2$
0	0.100	0.400
0.20	0.105	0.415
0.50	0.115	0.460
0.70	0.110	0.500
0.89	0.105	0.550

(a)  $\lambda = 0^\circ$

y/b	$b_1$	$b_2$
0.89	0.099	0.425
0.70	0.100	0.405
0.50	0.100	0.390
-0.50	0.120	0.500
-0.70	0.115	0.595
-0.89	0.115	0.700

(b)  $\lambda = 15^\circ$

y/b	$b_1$	$b_2$
0.89	0.110	0.355
0.70	0.110	0.355
0.50	0.110	0.355
-0.50	0.133	0.560
-0.70	0.134	0.680
-0.89	0.136	0.850

(c)  $\lambda = 30^\circ$

y/b	$b_1$	$b_2$
0.89 <sup>#</sup>	0.133	0.305
0.70	0.130	0.300
0.50	0.131	0.290
-0.50	0.165	0.700
-0.70	0.164	0.85
-0.89 <sup>#</sup>	0.160	1.200

(d)  $\lambda = 45^\circ$

**Table 2 Circulatory Response Coefficients, aspect ratio 6**

More significant variations are observed for the yawed wings. The magnitude of the exponential

terms can be considered constant except close to the tips of the  $\lambda = 45^\circ$  wing (indicated by <sup>#</sup> in Table 2) where a value of  $A_1 = 0.12$  was found to give a better fit. The coefficients controlling the phase of the response vary little close to the leeward tip, while at the windward tip there is significant variation of both coefficients.

### Discussion

The treatment of three-dimensional planform effects in modern indicial methods is described in some detail by Beddoes [Ref 10]. At the heart of the method is the assumption of spanwise independence of the indicial functions, or that the response function is essentially two-dimensional in character. Some local shaping of the lift curve slope, based upon classical steady theory, and the magnitude of the impulse response is employed to reflect the three-dimensional nature of the wing. The correlations presented by Beddoes suggest that the model is relatively robust in its treatment of pitching wings having widely varying planform characteristics. The model deals effectively with small aspect ratios, although comparisons of predicted and measured spanwise loading deteriorated towards the tip (this was attributed to a relatively crude discretization). For swept wings the method was found to be less reliable but provided acceptable agreement with the available experimental data. Overall the indicial method was demonstrated to provide improved predictions when compared to a lifting line code at significantly reduced computational expense. Although the improvement over lifting line analysis remains unexplained it is likely that the inclusion within the indicial model of the impulsive loading generated by the oscillating wing is important.

One of the drawbacks of the reported study was the concentration on tests conducted using swept back half models and swept wings obtained by a shearing transformation. In other words the model was validated for wings having only leeward projecting tips or tips that were aligned with the flow direction. The reported validation study did not consider the case of a windward projecting wing tip, and to the authors knowledge this deficiency has not been addressed in subsequent work.

As has been shown in the present study the unsteady aerodynamics of the leeward tip are much simpler than those of the windward tip and can, with acceptable accuracy, be reliably described using a constant response function provided that the coefficients are judiciously chosen. Thus the reported validation is wholly consistent with the results of the current investigation. In order to understand the implications of the current results further we must consider the case of a rotating wing.

Correlation studies of rotor flight test data with load prediction methods, such as those reported by Lau,

Louie, Sotiriou and Griffiths [Ref 23] and Hansford and Vorwald [Ref 24] implicate modelling of blade unsteady aerodynamics in poor prediction of aerodynamic performance, blade dynamics and vibratory loads. Sitaraman, Datta, Baeder and Chopra [Ref 25] have explored this issue in depth and identify problems with the calculated values of the advancing blade forces and moment as the principal causal factor.

In forward flight at modest to high advance ratios the advancing blade experiences a yawed flow resulting in the blade tip being projected into the oncoming freestream, see Fig. 1. From the results of the present investigation we expect that there will be significant three-dimensional influence on the local unsteady response that is not accounted for in current aerodynamic models. Although the amplitude of the resulting response is unlikely to be altered significantly, the more gradual development of the circulatory response will lead to important changes in phase which may help to explain the deficiencies of the indicial models in current use by the rotorcraft community.

### Conclusions

The indicial response of finite aspect ratio yawed wings was investigated using numerical solutions of the unsteady Euler equations. Computations were performed for a step forcing in pitch at low Mach number and modest incidence. Aspect ratio 3, 6 and 20 wings of rectangular planform and constant NACA 0012 cross-section were investigated at yaw angles of 0°, 15°, 30° and 45°. Based upon the computed data the following observations can be made:-

### Initial Response

It was found that the total initial response was independent of aspect ratio and yaw angle. Using simple sweep theory the computed data was shown to correlate with predictions made on the basis of simple acoustic considerations.

The presence of the tip vortex was found to change the local initial response close to the tips. Further inboard the initial lift response was correlated with piston theory. For the yawed wing the windward projecting tip was found to be more sensitive, as the vortical flows at the tip passed over the lower and upper surfaces of the wing before rolling up into a single vortex downstream of the trailing edge.

### Impulsive Decay

The initial rate of decay of the impulsive loading was found to be independent of planform for the configurations studied. However, at later times the local impulse responses were observed to diverge. The time interval between the initial forcing and divergence of the impulse responses was found to be correlated with distance from the blade tip

implicating the generation and propagation of spanwise acoustic waves as the responsible physical mechanism.

### Circulatory Response

Circulatory response functions based upon a modified exponential form of Wagner's function were extracted. The magnitude of the exponential terms was observed to be largely independent of aspect ratio and yaw away from the tips. The coefficients that control the phase of the response were found to be dependent upon the yaw angle. The coefficients were found to vary rapidly with distance from the tip at the windward tip, while at the leeward tip the variation was much smaller.

The implications of the observed three-dimensional response for prediction techniques employing two-dimensional response functions were considered. Although validation studies provide some confidence in the approach, it appears that the case of an oscillating wing tip projecting into the oncoming freestream had not previously been considered. The yawed flow experienced by the advancing blade at modest to high-flight velocities results in a windward projecting blade tip. Consequently the observed three-dimensional behaviour may play a role in explaining poor prediction of the advancing blade aerodynamics, dynamics and vibratory loading.

The results suggest that current industrial approaches for three-dimensional planforms are unreliable because of their reliance on two-dimensional indicial response functions. Further effort is required to understand and model the physical phenomena associated with the blade tip and the tip vortex.

### Acknowledgements

This work was undertaken with the financial support of the Engineering and Physical Sciences Research Council (EPSRC).

All of the reported calculations were performed on the Cambridge-Cranfield High-Performance Computing (CCHPC) System located at Cranfield University.

### References

1. Beddoes, T.S., 'Representation of Airfoil Behaviour', *Vertica*, Vol. 7 (2), pp. 183-197, 1983.
2. Beddoes, T.S., 'Practical calculation of unsteady lift', *Vertica*, Vol. 8 (1), pp. 55-71, 1984.
3. Leishman, J. G., 'Indicial lift Approximations for Two-Dimensional Subsonic Flow as Obtained from Oscillatory Measurements', *J. of Aircraft*, Vol. 30 (3) pp. 340-351, 1993.
4. Sitaraman, J., Baeder, J.D. and Iyengar, V., 'On the Field Velocity Approach and Geometric

- Conservation Law for Unsteady Flow Simulations', AIAA Paper 2003-3835, 16th AIAA Computational Fluid Dynamics Conference, 2003.
5. Shaw, S.T. and Qin, N., 'Calculation of compressible indicial response', *Aeronautical Journal*, Vol. 104 (1042), pp.665-673, 2000.
  6. Shaw, S.T. and Qin, N., 'Study of the aerodynamics of in-plane motion', *Proceedings of the IMECHE, Part G, Vol. 215*, pp.89-104, 2001.
  7. Gaitonde, A.L. and Jones, D.P., 'The use of Pulse Responses and System Reduction for 2D Unsteady Flows Using the Euler Equations', *Aeronautical Journal*, Vol. 106 (1063), pp483-492, 2002.
  8. Beedy, J., Barakos, G., Badcock, K., and Richards, B., 'Non-linear analysis of stall flutter based on the ONERA aerodynamic model', *Aeronautical Journal*, Vol. 107(1074), pp 495-509, 2003.
  9. Beddoes, T.S., 'A wake model for high-resolution air-loads', *US Army/American Helicopter Society Conference on Rotorcraft Basic Research*, Raleigh, 1985.
  10. Beddoes, T.S., 'Two- and three-dimensional indicial methods for rotor dynamic air-loads', *AHS Specialists meeting on rotorcraft dynamics*, Arlington, 1989.
  11. Beddoes, T.S., 'A 3-D Separation Model for Arbitrary Planforms', *47th Annual Forum of the American Helicopter Society*, 1991.
  12. Beddoes, T.S., '3D Dynamic Stall - Correlation Study', *Westland Helicopter Internal Report, Aero-Tech Note Gen/166*, 1991.
  13. Singh, R., and Baeder, J.D., 'The Direct Calculation of Indicial Lift Response of a Wing Using Computational Fluid Dynamics', *J. of Aircraft*, Vol. 35 (4), pp.465-471, 1997.
  14. Sitaraman, J. and Baeder, J.D., 'Computational-Fluid-Dynamics-Based Enhanced Indicial Aerodynamic Models', *J. of Aircraft*, Vol. 41 (4) pp. 798-810, 2004.
  15. Sperijsse, S. P., 'Multi-grid Solution of the Steady Euler Equations', *Ph.D. Dissertation, Centrum voor Wiskunde en Informatica, Amsterdam*, 1987.
  16. Osher, S. and Solomon, F., 'Upwind difference schemes for hyperbolic systems of conservation laws', *Mathematics of computation*, Vol. 38 (158), pp. 339-374.
  17. Shaw, S.T., 'Numerical study of the unsteady aerodynamics of helicopter rotor aerofoils', *PhD Thesis, Cranfield University*, 1999.
  18. Van Leer, B., 'Towards the ultimate conservative difference scheme V: A second order sequel to Godunov's method', *J. Computational Physics*, Vol. 32, pp.101-136, 1979.
  19. Karypis, G. and Kumar, V., 'Multi-level k-way partitioning scheme for irregular graphs', *J. of Parallel and Distributed Computing*, Vol. 48 (1), pp. 96-129, 1998.
  20. Roache, P.R., 'Verification and validation in computational science and engineering', *Hermosa publishing*, 1998.
  21. Lomax, H., 'Indicial aerodynamics', *AGARD Manual of Aeroelasticity, Part 2, Chapter 6*, 1960.
  22. Tobak, M., 'on the use of indicial function concept in the analysis of unsteady motions of wings and wing-tail combinations', *NACA Report R-1188*, 1954.
  23. Lau, B.H., Louie, A.W., Sotiriou, C.P. and Griffiths, Nicolas, 'Correlation of the Lynx-XZ170 flight test results up to and beyond the stall boundary', *Proceedings of the 49th Forum of the American Helicopter Society*, 1993.
  24. Hansford, R.E. and Vorwald, J., 'Dynamics workshop on rotor vibratory loads prediction', *J. American Helicopter Society*, Vol. 43(1), pp.76-87, 1998.
  25. Sitaraman, J., Datta, A., Baeder, J.D. and Chopra, I., 'Fundamental understanding and prediction of rotor vibratory loads in high-speed forward flight', *Proc. 29th European Rotorcraft Forum*, 2003.